CMS Internal Note

The content of this note is intended for CMS internal use and distribution only

Azimuthal Anisotropy in Heavy Ions Collisions with CMS Tracker

G. Kh. Eyyubova, V. L. Korotkikh, I. P. Lokhtin, S. V. Petrushanko, L. I. Sarycheva, A. M. Snigirev,

Skobeltsyn Institute of Nuclear Physics, Moscow State University, 119992 Moscow, Russia

D. Krofcheck

The University of Auckland, Private Bag 92019 Auckland Mail Centre, Auckland 1142, New Zealand

Abstract

The azimuthal anisotropy of charged particles in heavy ion collisions is a very sensitive signature of quark-gluon plasma evolution at early time stages. An analysis based on a full CMS detector simulation of HYDJET Pb+Pb events shows that the event plane resolution achieved with the CMS Tracking System is close to the resolution obtained on the generator level, and somewhat better than the resolution obtained with the CMS calorimeters. The transverse momentum and rapidity dependencies of the elliptic flow coefficient v_2 can be reconstructed in the CMS Tracker with high accuracy.

1 Introduction

The azimuthal anisotropy of charged particles is one of the most important features of the dense quark-gluon plasma (QGP) in heavy ion collisions. In non-central collisions between two nuclei the beam direction and the impact parameter define a reaction plane for each event. The observed particle yield versus azimuthal angle with respect to the event-by-event reaction plane gives information on the early collision dynamics [1, 2]. An initial overlap region has an "almond" form at non-zero impact parameter. If the produced matter interacts and thermalizes, pressure is built up within the almond shaped region leading to anisotropic pressure gradients. This pressure pushes against the outside vacuum and the matter expands collectively. The expansion is fastest along the largest pressure gradient, i.e. along the shortest axis of the almond. The result is an anisotropic p_T distribution in the detected particles. One can expand this p_T distribution in a Fourier series. The second coefficient of the expansion v_2 is often called the elliptic flow and it is expected to be the dominant contribution.

The elliptic flow was measured at low and high energies (SPS-RHIC) (Fig.1) [4]. A ratio of elliptic flow to spatial eccentricity achieves the value of 0.2 at RHIC energies which is consistent with the hydrodynamical limit.

In the RHIC experiments for Au+Au collisions at 200A GeV [5, 6, 7] $v_2(p_T)$ increases with p_T up to $p_T \simeq 1$ GeV/c and then it is saturated. Both the increase and the saturation value of v_2 are described by the hydrodynamic model [8]. At higher $p_T > 1$ GeV/c it is necessary to introduce other model descriptions, including the energy loss of hard partons in a dense medium. The change of regime in p_T dependence in the intermediate region coincides with the beginning of the jet saturation region. The pseudorapidity dependence $v_2(\eta)$ is also not described well by pure hydrodynamic models. The $v_2(\eta)$ has a maximum at $\eta = 0$ and falls with increasing $|\eta|$, in contrast to an approximate plateau for $|\eta| < 2$ in the hydrodynamics. However using appropriate initial conditions for hydrodynamics and accounting for hadronic rescattering can improve the description of $v_2(\eta)$ [9].

The capabilities of the CMS calorimetric system to study elliptic energy flow were analyzed in [10]. It was shown that the calorimetric system is well suited to measure energy flow and jet azimuthal anisotropy at high p_T.

This note is dedicated to studying the capabilities of CMS tracker to measure the particle azimuthal anisotropy in the intermediate p_T region.

2 The CMS Tracker

2.1 Geometrical layout

The CMS tracker is located, together with the electromagnetic and hadronic calorimeters, inside a 4 T solenoidal magnetic field. It consists of a pixel detector, providing 2 to 3 hits per track, and a Silicon Strip detector providing 10 to 14 hits. There are about 10 million microstrips and 40 million pixels.

The pixel detector is composed of 3 cylindrical layers and 2 pairs in the end-caps, such that 3 points are measured per track for $|\eta| < 2.2$. In the barrel ($|\eta| < 1.5$), the three layers are located at radii of 4.3 cm, 7.5 cm, 10.2 cm, and in the endcaps ($1.5 < |\eta| < 2.4$) the two pairs of disks are located at $|z| = 34.5$ cm, $|z| = 46.5$ cm. With the pixel size of $100 \times 150 \mu$m the hit resolution is approximately 10 μm in $r - \varphi$, and 20 μm in $r - z$.

The Silicon Strip detector has the following parts. The Tracker Inner Barrel (TIB) is composed of 4 cylindrical layers, enclosed by 3 pairs of disks (Tracker Inner Disks, TID). It is then followed by 6 cylindrical layers of the Tracker Outer Barrel (TOB). The Tracker Endcaps (TEC) are made of 9 pairs of disks. The strip length ranges from 9 cm in the inner part to 21 cm in the outer part, and pitches range from 80 to 205 μm. Some of the layers and rings of disks are instrumented with double sided modules, where the detectors are glued back-to-back with a stereo angle of 100 mrad.
The schematic layout and geometrical coverage of the tracker is shown in Fig.2.

2.2 Track reconstruction

The baseline algorithm for track reconstruction [11] in CMS is the Combinatorial Kalman Filter. After track hits have been found the track reconstruction proceeds via the following four steps: trajectory seeding, pattern recognition, trajectory cleaning, and track fitting and smoothing.

The Kalman filter proceeds iteratively from the seed layer and includes the information from the successive acceptable layers one by one. With each included layer, track parameters are better constrained. In the extrapolation of the trajectory from layer to layer, the effects of energy loss and multiple scattering are taken into account.

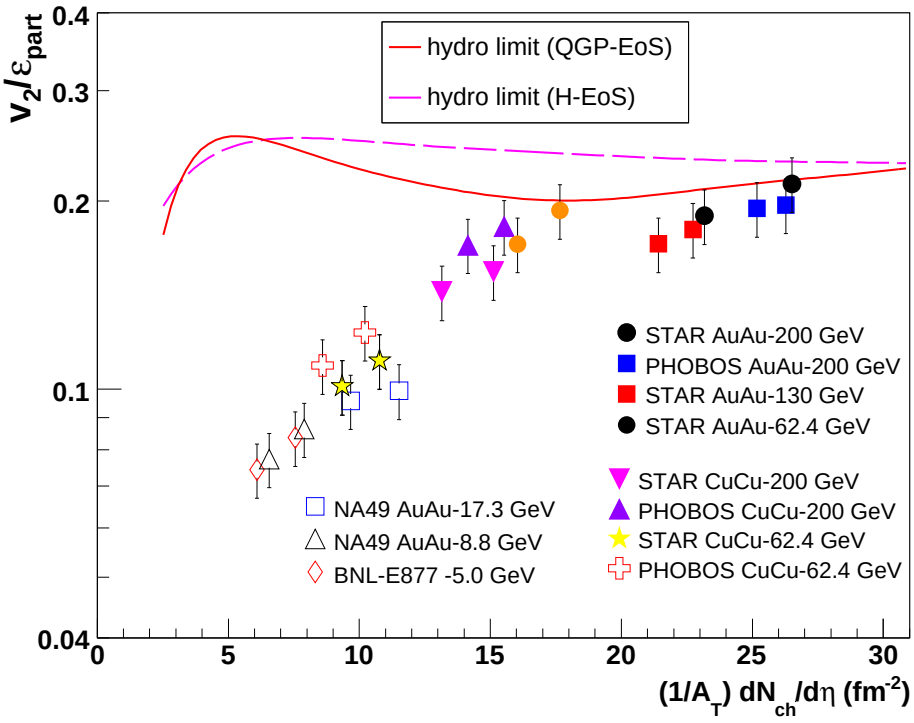

Figure 1: The ratio of elliptic flow to spatial eccentricity as a function of the hadron rapidity density normalized by the reaction overlap area $A_\perp$, compared to the hydrodynamical limit for a fully thermalized system with quark-gluon plasma or hadron equaton of state. This Figure is taken from [3].

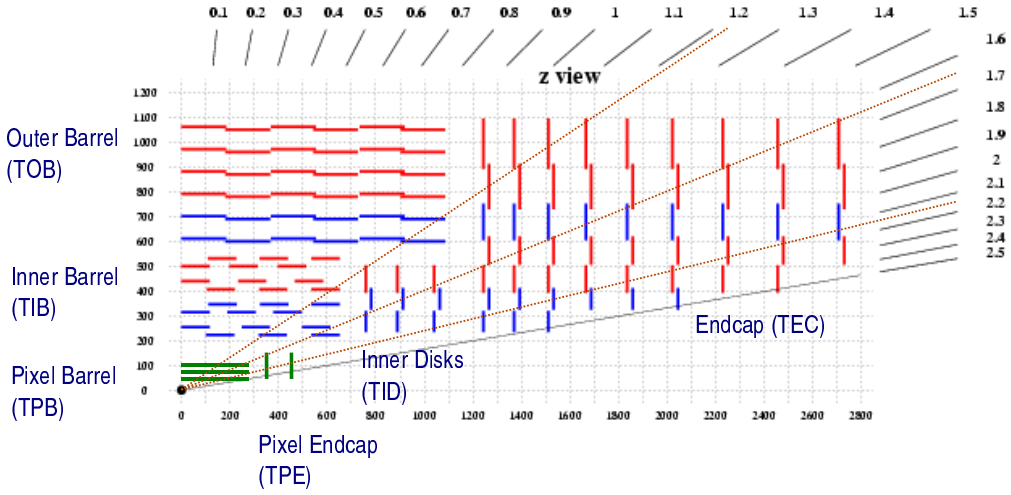

Figure 2: Illustration of the CMS Tracker layers, one quarter of the full tracker in rz view [12].

The global track finding efficiency in p-p collisions for muons is about 98% over most of the tracker acceptance. For hadrons the reconstruction efficiency is between 75 and 95% [12]. For nucleus-nucleus collisions the efficiency is lower (70% - 80%) because of the high multiplicity and the larger number of fake tracks [13].

3 Reconstruction of charge particle distributions

This study is based on simulations of heavy ion collisions using the HYDJET event generator [14]. A sample of 1000 Pb-Pb events at impact parameter $b = 9$ fm was utilized. At this centrality the number of reconstructed tracks per event is about 250. Some settings were used to reconstruct tracks (i.e. the number of hits on a track > 12, the track fit probability > 0.01) and a cut on $p_T > 0.9$ GeV/c was set in both simulated and reconstructed events.

3.1 Multiplicity

The azimuthal and η charge particle distribution for simulated and reconstructed events is shown in Fig.3, the reaction plane angle in the simulated events was equal to zero.

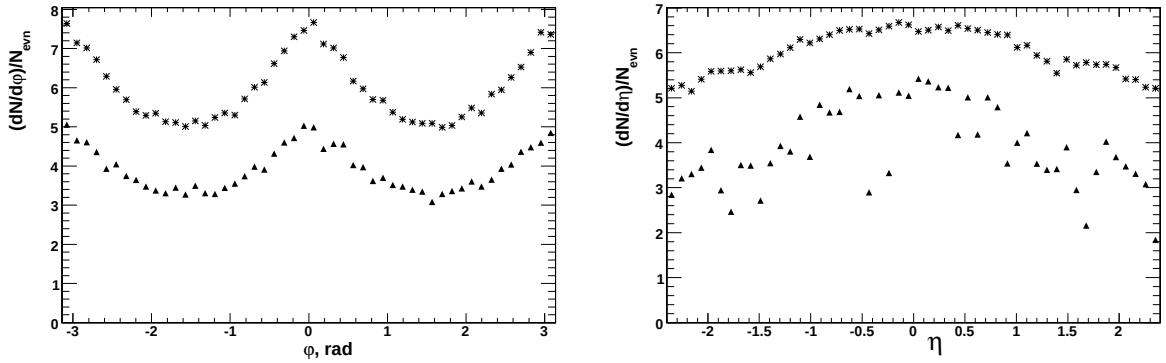

Figure 3: Left plot:Simulated (stars) and reconstructed (triangle) azimuthal charge particle distribution at impact parameter b=9 fm, right plot: η distribution.

An anisotropic azimuthal pattern is seen at both the generated and track reconstructed levels.

The p_T charged particle distribution for simulated and reconstructed events and the ratio of reconstructed and simulated p_T distributions are shown in Fig.4.

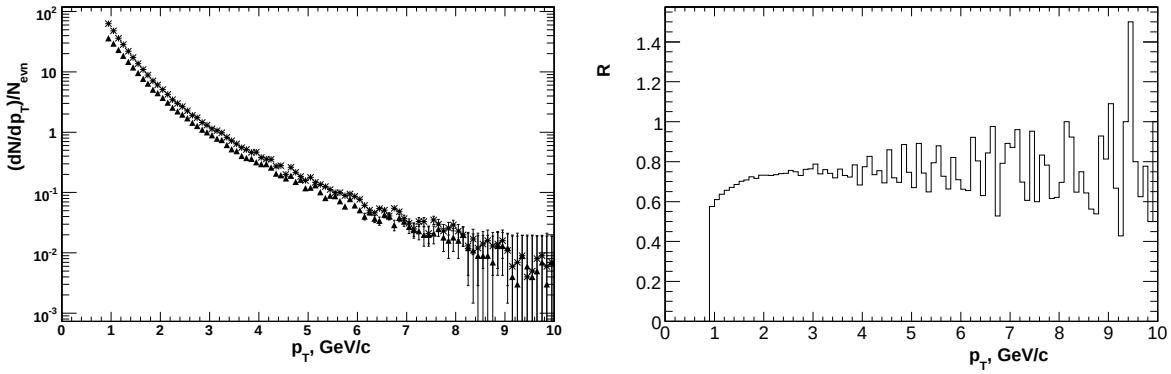

Figure 4: Left plot: p_T distribution of reconstructed (triangles) and simulated (stars) tracks, right plot: ratio of reconstructed and simulated p_T distributions at impact parameter b=9 fm.

3.2 Reconstruction of nuclear reaction plane

The reaction plane angle, Ψ_n, can be determined from the measured n-th harmonics via the standard method [15, 10]:

$$\tan n\Psi_n = \frac{\sum\limits_i w_i \sin(n\varphi_i)}{\sum\limits_i w_i \cos(n\varphi_i)} \tag{1}$$

where φ_i is the azimuthal angle of the i-th particle and w_i is the weight. The sum runs over all particles.

The accuracy of event plane determination is mainly sensitive to two model factors: the strength of elliptic flow, and the event multiplicity. To illustrate the dependence of the accuracy of event plane determination on event centrality, sets of 1000 HYDJET Pb+Pb events were created at the generator level for each of twelve centrality bins covering the range of impact parameters from $b = 0$ to $b = 2R_A$ (R_A is a nuclear radius). HYDJET events both with and without jet quenching were generated. Stable particles with pseudorapidity of $|\eta| < 3$ (CMS barrel+endcap calorimetry acceptance) were considered for the event plane analysis for $n = 2$ and $\omega_i = p_{Ti}$. An additional cut

of $p_T^{\rm ch} > 0.8$ GeV/c on charged particle transverse momentum was applied in order to take into account the effect of charged particles with smaller p_T values. Such particles cannot reach the calorimeter surface in the 4 T CMS magnetic field.

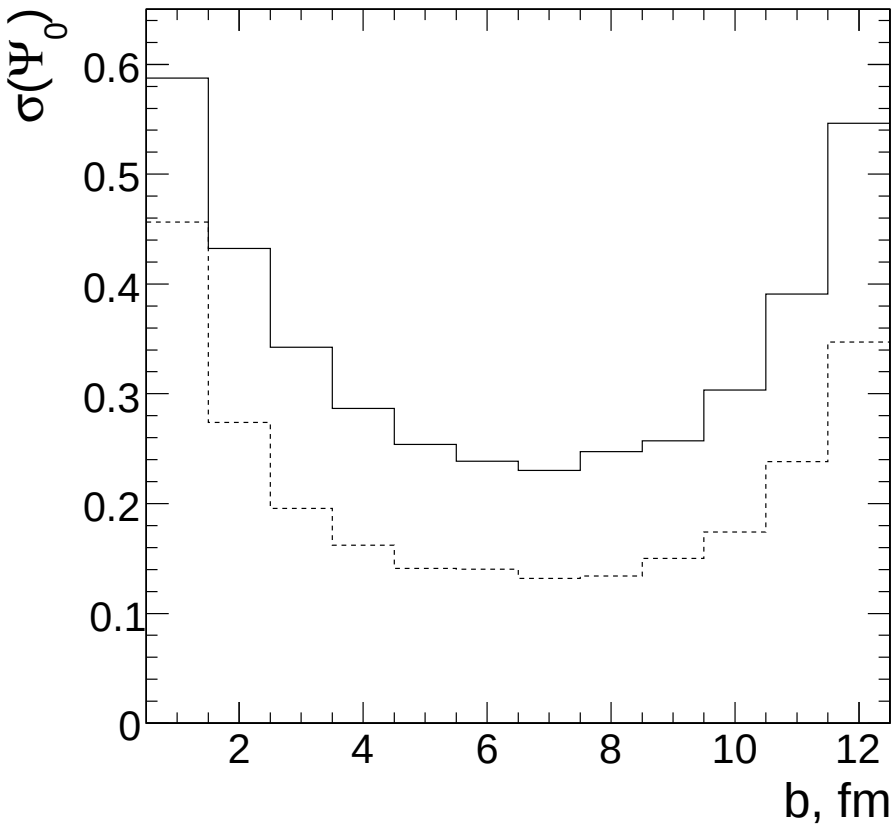

Figure 5: Event plane resolution $\sigma(\Psi_0)$ as a function of impact parameter in Pb+Pb collisions with "standard" (solid histogram) and "high" (dashed histogram) multiplicities (jet quenching off).

Figure 5 shows the calculated resolution $\sigma(\Psi_0)$, defined here as the width of a Gaussian fit of the distribution over the difference between the generated, Ψ_0, and calculated, Ψ_2, azimuthal angles of the reaction plane (1), as a function of impact parameter in Pb+Pb collisions (jet quenching off). The interplay of multiplicity and anisotropic flow in opposite centrality directions for central and semi-central collisions results in the best resolution obtained at impact parameters on the order of the nuclear radius, $b \sim R_A$. In order to demonstrate the influence of multiplicity on the accuracy of event plane determination, the resolution for "high" multiplicity events (obtained by increasing the multiplicity of the soft part of the event by a factor of 2, i.e. with the total multiplicity of soft part ~ 52000 in central Pb+Pb collisions) was also calculated. Increasing the soft multiplicity by a factor of 2 results in an improvement of resolution by a factor ~ 1.7 with a rather weak dependence on the event centrality.

Introducing jet quenching into the model results in a rise of event multiplicity and the generation of some additional elliptic flow in the high-p_T region. The estimated improvement on the event plane resolution in this case is on the level of 20-25% for both "standard" and "high" multiplicities.

The distributions of reaction plane angle Ψ_2, obtained by using Eq. 1 with $n = 2$ and $w_i = 1$ for 1000 HYDJET events at impact parameter b=9 fm are shown in Fig.6. The resolution of the angle for simulated events is equal to $\sigma_{\rm sim} = 0.27$. A comparison of the resolutions with Tracker and Calorimeters is in Table 1.

Table 1: Resolution of reaction plane reaction.

Detector	$\sigma_{\rm rec}$
ECAL+HCAL(Barrel+Endcaps)	0.37
Tracker	0.31

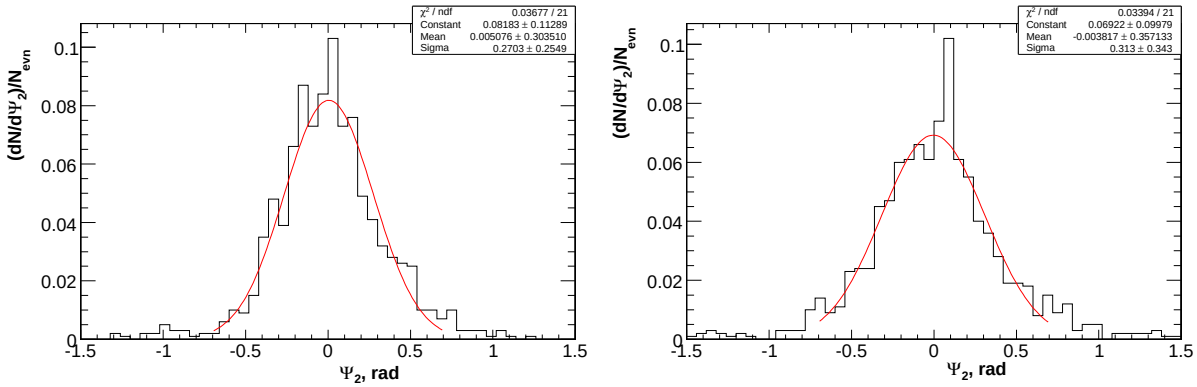

Figure 6: Distribution of the event plane angle for simulated (left) and reconstructed (right) events

4 v_2 calculation

We assume, according to the hydrodynamic model, that in the expansion of the particle distribution in a Fourier series the v_2 term has the dominant contribution and the azimuthal distribution is described by the elliptic form:

$$\frac{dN}{d\varphi} = \frac{N_0}{2\pi}[1 + 2v_2 \cos 2(\varphi - \Psi_R)] \tag{2}$$

where Ψ_R is the event plane angle, N_0 stands for full multiplicity. Then v_2 is the average over particles of $\cos(2(\varphi - \Psi_R))$:

$$v_2 = < \cos(2(\varphi - \Psi_R)) > \tag{3}$$

Here we apply two methods to calculate v_2-coefficient. The first one uses the reaction plane angle determination mentioned above, and the second one does not involve the event plane angle determination. The basic idea of the latter method is that the v_2 coefficient can be expressed in terms of particle correlations [15]. As shown below, these two methods yield equivalent results for v_2.

Also, we calculate the v_2 coefficients from fitting the $dN/d\varphi$-distribution in each event using Eq. (2) with the following free parameters: N_0, v_2 and Ψ_R.

4.1 v_2 with reaction plane angle

The distributions of v_2 coefficients over 1000 events, calculated with reaction plane angle by using Eq. (1) is shown in Fig. 7.

The variance of v_2, defined as $\sigma(v_2)$, is shown in Table 2.

4.1.1 p_T and η dependence

The p_T and η dependence of the elliptic flow are shown in Fig.8 and Fig.9.

4.2 v_2 calculation by particle correlation

The method of v_2 calculation without event plane angle reconstruction was suggested in [15]. In the case when there are no other particle correlations except those due to flow, the coefficient of azimuthal anisotropy can be determined using a two-particle azimuthal correlator.

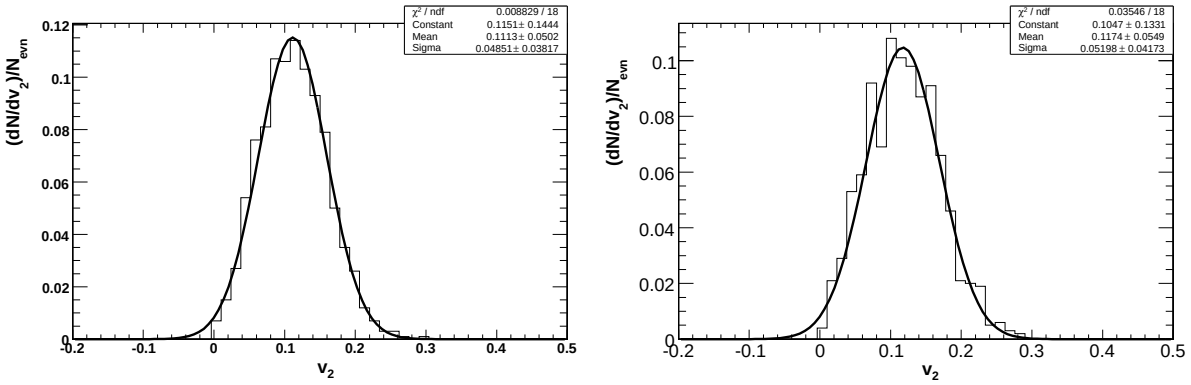

Figure 7: Distribution of v_2-coefficient in simulated (left) and reconstructed event (right) with the reaction plane angle obtained by Eq. (1)

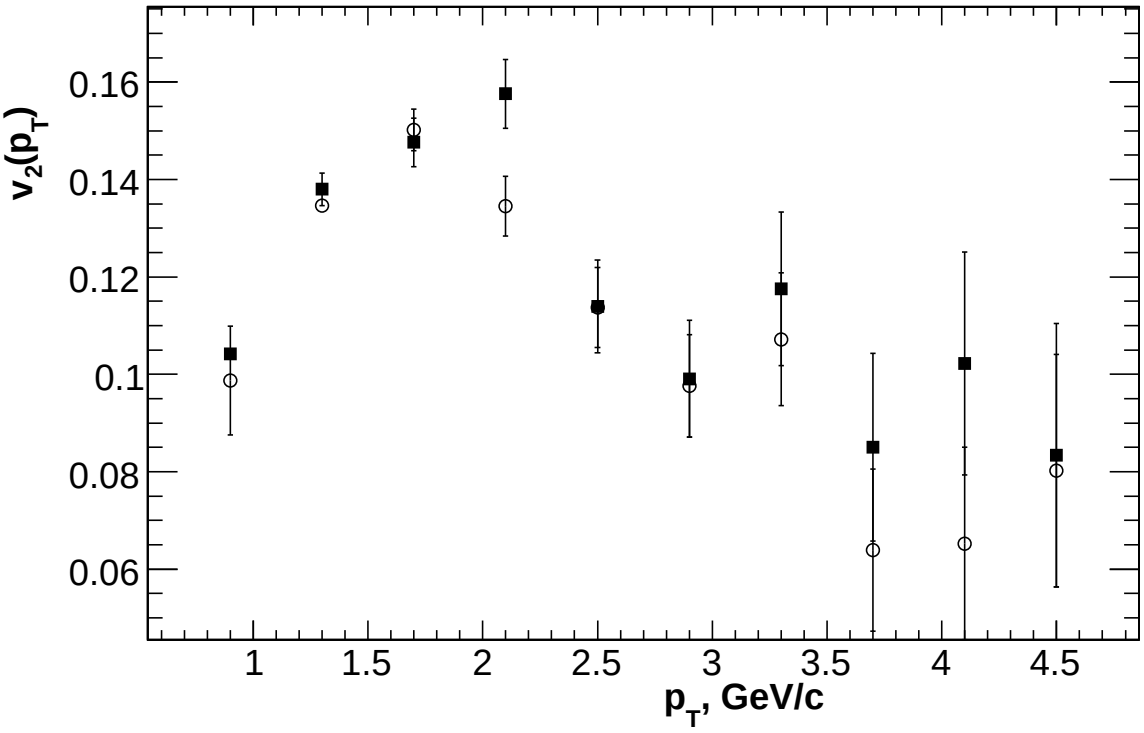

Figure 8: p_T dependence. Cubes are reconstructed values of v_2, open points are simulated values of v_2

$$v_2^2 =< \cos 2(\varphi_1 - \varphi_2) > \tag{4}$$

The variance of v_2 is in Table 2. A comparison of the two methods, Eq. (3) and Eq. (4) respectively, is shown as a ratio $v_2^{\rm rec}/v_2^{\rm sim}$. The coefficient v_2 from the reconstructed events with the CMS Tracker differs approximately % 5 from the simulated events for the two methods.

This ratio is compatible with unit within statistical errors.

Finally, the distribution of v_2-coefficients, extracted from fitting of $dN/d\varphi$-distribution in each event by Eq. (2), is shown in Fig. 10.

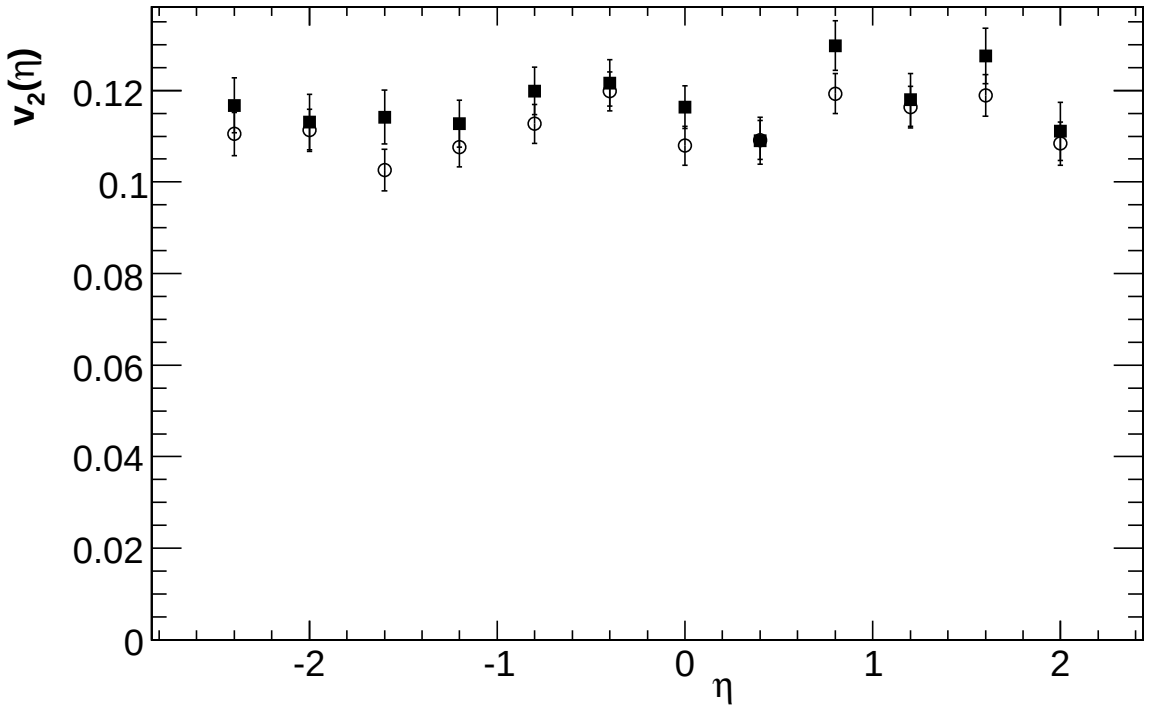

Figure 9: η dependence. Cubes are reconstructed values of v_2, open points are simulated values of v_2

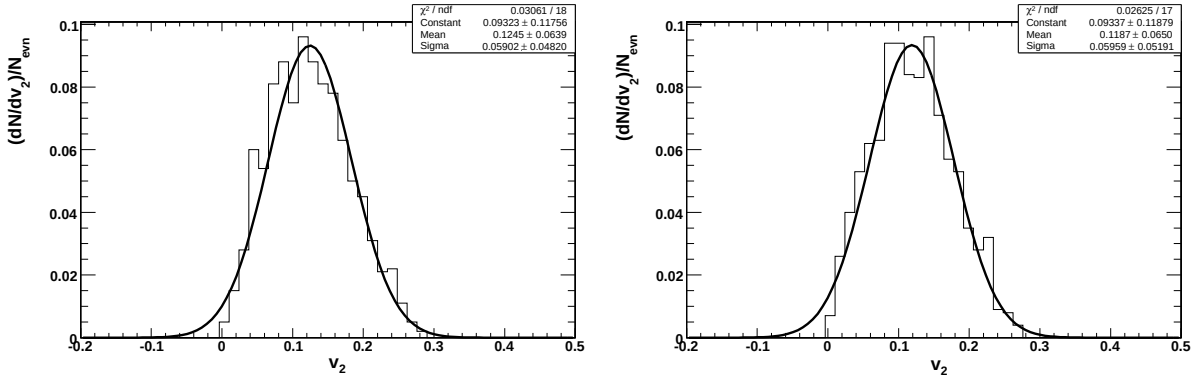

Figure 10: Distribution of v_2-coefficients in simulated (left) and reconstructed events (right) from fitting by Eq. (2)

5 Conclusion

The capability of CMS Tracking System to measure azimuthal anisotropy of charged particles in heavy ion collisions has been analyzed for the first time. The azimuthal flow was calculated here by two methods. The first method was based upon the determination of the reaction plane, and the second was based on particle correlations without a determination of the reaction plane. It was shown that these two methods give similar results, because they are based on the same suggestion that the azimuthal distribution of particles is described by the elliptic form.

The analysis, based on a full detector simulation of HYDJET Pb+Pb events, shows that the event plane resolution achieved by using the CMS Tracker is close to the resolution obtained on the generator level, and is somewhat better than the resolution obtained with the CMS calorimeters.

The transverse momentum and rapidity dependences of the elliptic flow coefficient can be reconstructed using the CMS Tracker with high accuracy.

To conclude, let the areas for future related studies to be outlined. The sensitivity to non-flow effects in the two-particle azimuthal correlation methods motivated the development of new techniques, which make use multi-

Table 2: Ratio of v_2 for reconstructed and simulated events, and the v_2 variance.

Method	$v_2^{\rm rec}$	$\sigma(v_2)$	$v_2^{\rm rec}/v_2^{\rm sim}$
$< \cos 2(\varphi - \Psi_R) >$	0.1174	0.051	1.055
$\sqrt{(< \cos 2(\varphi_1 - \varphi_2) >)}$	0.1174	0.052	1.055
v_2 from fitting	0.1187	0.059	0.95

particle azimuthal correlations by performing a cumulant expansion where the collective source of correlations can be disentangled from other sources. Thus it will be useful to compare the four-particle and two-particle cumulant methods for CMS installation. Another analysis that would be interesting would be looking at the capability of CMS Tracker to measure also non-second coefficients of a Fourier expansion of the particle p_T-distribution, which can reflect important dynamics of the reaction. In particular, $v_4(p_T)$ near mid-rapidity and $v_1(p_T)$ at the most forward rapidity covered by the tracker may be of the interest.

6 Acknowledgments

The authors thank David d'Enterria, Olga Kodolova, Christof Roland, Stephen Sanders, Irina Vardanyan and Boleslaw Wyslouch for fruitful discussions.

References

[1] J.-Y. Ollitrault, Phys. Rev. **D46**, 229 (1992).

[2] H. Sorge, Phys. Rev. Lett. **82**, 2048 (1999).

[3] D. d'Enterria, arXiv:nucl-ex/0611012.

[4] S. Mainly (PHOBOS Collaboration), Nucl. Phys. **A774**, 523 (2006).

[5] K. Adcox et al.(PHENIX), Nucl. Phys. **A757**, 1 (2005).

[6] B. Back et al.(PHOBOS), Nucl. Phys. **A757**, 28 (2005).

[7] J. Adams et al.(STAR), Nucl. Phys. **A757**, 102 (2005).

[8] P. Huovinen et al., Phys. Lett. **B503**, 58 (2001).

[9] T. Hirano et al., Phys. Lett.**B636**, 299 (2006)

[10] I.P. Lokhtin, S.V. Petrushanko, L.I. Sarycheva, A.M. Snigirev CMS Note 2003/019, 2003.

[11] W. Adam et al., CMS Note 2006/041 (2006).

[12] F. -P. Shilling (CMS Collaboration), arXiv:physics/0610005, 2006

[13] G. Roland, CMS Note 2006/031 (2006)

[14] I.P.Lokhtin and A.M.Snigirev, Eur. Phys. J. C **46** (2006) 211.

[15] S. A. Voloshin and Y. Zhang, Z. Phys. C **70** (1996) 665.